Draft version: April 8, 2017

Proposed sections in the introduction:

1. Exoplanet Observations – Dominant detection methods (Transit, RV), basic statistics of exoplanets discovered by Kepler Space Telescope.
2. Planet Formation – MMSN, Core accretion/GI models, Planetesimal Formation.
3. Planetary Dynamics – Mean Motion Resonance, (planetesimal and gas) Migration, Stability.
4. Numerical Integration – Hamiltonian Dynamics, integrator types (hybrid, symplectic, high order), coordinate systems (jacobi, heliocentric, whds).
5. Tie intro to thesis

1. Exoplanet Observations

1.1. Detection Methods

1.1.1. Radial Velocity

A planet and star will orbit around their common centre of mass, and since all stars emits light a periodic wobble can be observed. From the conservation of energy and angular momentum the radial velocity of a star due to a planetary companion can be calculated according to (Beaugé et al. 2007):

$$V_r = K \cdot [\cos(\nu(t) + \omega) + e \cdot \cos(\omega) + \gamma] \tag{1}$$

where K is the semi-amplitude:

$$K = \frac{m_p \sin(i)}{m_* + m_p} \frac{2\pi a}{P\sqrt{1 - e^2}} \tag{2}$$

a is the semi-major axis of the planet, P is the orbital period, m_p is the planet mass, m_* is the stellar mass, i is the inclination of the orbital planet, e is the eccentricity of the planet, $\nu(t)$ is the true anomaly, ω is the argument of periastron, and γ is the stellar drift in velocity. Since the probability of detecting a planet is related to K, Equation 2 reveals that radial velocity is best at detecting massive planets on short orbits.

In theory, these equations will yield the orbital parameters of the planet (mass, eccentricity, orbital period, etc.). In practice, there are some uncertainties associated with this method. For example, successfully extracting orbital parameters requires accurate and precise knowledge of the stellar mass, which is typically difficult to obtain (e.g. Brown et al. 2011). Furthermore, only a lower limit $m\sin(i)$ estimate on planet mass can be calculated unless the inclination relative to Earth's line of sight is known. In addition, the radius of the planet cannot be calculated from the radial velocity method, precluding any information about size and density.

When multiple planets orbit a star the radial velocity signal becomes more complex, though it is still periodic in nature (assuming orbital stability). Assuming that the planets are well-separated such that their mutual gravitational interactions are weak, the radial velocity of the star can be approximated as the sum of planetary Keplerian orbits:

$$V_r = \gamma + \sum_{i=1}^{n_p} K_i \cdot [\cos(\nu_i(t) + \omega_i) + e_i \cdot \cos(\omega_i)] \tag{3}$$

where n_p is the number of planets in the system. If however the planet-planet gravitational interactions are strong, Equation 3 is invalid and must be replaced with a more careful numerical treatment.

1.1.2. Transit Method

When a planet passes (or transits) in front of its host star, a portion of the star's emitted flux F will be blocked. The fraction of blocked flux is proportional to relative areas of the star and planet:

$$\frac{\Delta F}{F} \propto \left(\frac{r_p}{r_*}\right)^2 \tag{4}$$

where r_p and r_* are the planet and stellar radii, respectively. In addition, the probability of a transiting planet P_t is inversely proportional to its semi-major axis:

$$P_t = \frac{r_*}{a_p} \tag{5}$$

Thus, from Equations 4 and 5 we see that large and short-period planets are preferentially detected by the transit method.

The first transiting planet was detected by Henry et al. (1999) and independently by Charbonneau et al. (2000). Since then, the transit method has become the most successful detection technique, with over 2,700 confirmed planets to date (NASA Exoplanet Archive 2017), with most of these discoveries coming from the *Kepler Space Telescope* (hereafter *Kepler*). The next most successful detection technique is the radial velocity method (Section 1.1.1) with over 600 confirmed planets to date (NASA Exoplanet Archive 2017).

From the transit method one can determine the period and radius of the planet. In addition, the atmospheric properties of exoplanets can also be determined (Kreidberg et al. 2014; Tsiaras et al. 2016; Stevenson et al. 2016). In total, the transit method is able to provide essential information about the composition, formation and habitability of a planet. However, the transit method is not without its weaknesses. For example, important parameters for dynamical analysis, like eccentricity and mass, cannot be determined for individual systems via the transit method. In addition, false positives from eclipsing binaries and background targets are a huge source of contamination (Fressin

et al. 2013), and confirmation via a different method is often required. Smaller planets and/or planets belonging to multi-planet systems are much less likely to be false positives than large, single planets (Fressin et al. 2013).

1.2. Statistics of Kepler Planets

The *Kepler* mission is the most successful planet-finding mission to date, providing scientists for the first time a large population of planets orbiting other stars. Due to the selection bias of the transit method (see Section 1.1.2), most of these planets have periods of less than 50 days and are much larger than Earth. However, sufficient detection across the full range of Earth-Jupiter sized planets has allowed scientists to calculate the occurrence of planets around other stars in our galaxy.

Two seminal works analyzing the *Kepler* population are Fressin et al. (2013) and Petigura et al. (2013). Fressin et al. (2013) found that the global false positive rate of the *Kepler* data is roughly 10%, the radius distribution peaks at mini-Neptune ($2 < r_p/r_\oplus < 2.8$, $r_\oplus$ is the radius of Earth) sized planets, and the occurrence of Neptune and Jupiter sized planets is significantly lower than the occurrence of $r_p/r_\oplus < 2.8$ sized planets. Using a very carefully vetted data sample, Petigura et al. (2013) found a similar result as Fressin et al. (2013), i.e. that the radius distribution peaks at mini-Neptune and the occurrence of Neptune and Jupiter sized planets is much lower.

The calculation for planet occurrence is usually performed by binning the planets in r–P space (where r is planet radius and P is planet period), and calculating planet occurrence for each bin. The occurrence $f(P_i, r_j)$ of planets in bin (i, j) for a population of planets is:

$$f(P_i, r_j) = \frac{1}{N_*} \sum_{k}^{n_p(i,j)} \left(\frac{a_k}{r_{*,k}} \frac{1}{\epsilon(i,j)} \right) \tag{6}$$

where N_* is the total number of stars surveyed in the sample, $n_p(i,j)$ are the number of planets falling into bin (i,j), $\frac{a_k}{r_{*,k}}$ is the geometric correction factor to account for missed non-transiting planets (inverse of Equation 5) and $\epsilon(i,j)$ is the detection completeness of bin (i,j) to account for missed transiting planets due to low signal-to-noise.

Of the ingredients that go into a Equation 6, the most difficult quantity to accurately measure is the detection completeness. Unlike Fressin et al. (2013) who used Combined Differential Photometric Precision (CDPP) values to estimate the detection completeness of known planets, Petigura et al. (2013) instead performed an injection and recovery of simulated light curves to calculate the detection completeness. Although injection and recovery of simulated light curves is certainly a more accurate and sophisticated algorithm to calculate detection completeness, Fressin et al. (2013) found that CDPP estimates were robust and could lead to accurate predictions.

One critical aspect of planet occurrence that Fressin et al. (2013) and Petigura et al. (2013) failed to incorporate into their calculations was the large error bars present in the *Kepler* data. The mean planetary radius error in the Batalha et al. (2013) *Kepler* dataset is 30%, meaning that, within 3 standard deviations a super-Earth sized planet could actually be Neptune or Earth-sized. These errors primarily stem from the fact that the radii of *Kepler* stars are not well known (Brown et al. 2011), with a mean radius error also about 30%. With such large error bars present in the *Kepler* data, ignoring them can significantly affect the resulting occurrence distribution.

2. Planet Formation

2.1. Minimum Mass Solar Nebula (MMSN) and Snowline

The initial conditions of a new solar system is still unknown, but missions like the Atacama Large Millimeter/submillimeter Array (ALMA) have begun to answer this question, imaging circumstellar disks around young stellar objects like HL Tau (**?**). In total, about 80 circumstellar and debris disks have been observed to date (e.g. Schneider et al. 2014; Choquet et al. 2016), revealing unexpected features like concentric rings sculpted by large planets (Tamayo et al. 2015). However, even 10 years ago little was known about the birth of young planetary systems. Hayashi (1981) and Weidenschilling (1977b) provided the first benchmarks for the initial mass of the Solar System by assuming a rocky core for all planets and calculating the initial surface density distribution $\Sigma(d)$ as a function of distance d required to produce the masses of the planets:

$$\Sigma(d) = \Sigma_0 \left(\frac{d}{1\text{AU}}\right)^{-3/2} \tag{7}$$

where $\Sigma_0 = 1700$g/cm^2. This initial surface density distribution has been dubbed the "minimum mass solar nebula" (MMSN), and is a benchmark for current studies.

Another critical property of circumstellar disks is the location of the snowline. According to conventional theory (), the snowline marks the region beyond which water turns to ice and Jovian planets can form. From Hayashi (1981), the benchmark temperature profile $T(d)$ for the Solar System is:

$$T(d) = T_0 \left(\frac{r}{1\text{AU}}\right)^{-1/2} \tag{8}$$

where $T_0 = 280$K. In this model, the radius at which the temperature drops to below freezing is $\sim 2.7AU$. More recent models that include more detailed models of radiative transfer and heating via accretion show that the primordial snow line in our Solar System could have been as close as 1 AU (Sasselov & Lecar 2000).

2.2. Planetesimal Formation

Before planets can form, kilometer-sized planetesimals must first be plentiful. There are two main pathways hypothesized for forming planetesimals – coagulation (core-accretion) and gravitational instability. In the coagulation model of planetesimal formation, pairwise collisions between sticky dust particles lead to steady growth up to meter sized objects and beyond (Weidenschilling 1977a; Armitage 2010). However, mean collision velocities are strongly coupled to size, and are largest for meter-size bodies (Weidenschilling 1977a), leading to destructive collisions (Blum & Wurm 2008) and hindering planetesimal formation. In addition, meter-sized objects in the protoplanetary disk will typically drift into the central star within $\sim 10^3$ years due to strong gas coupling (Weidenschilling 1977a), requiring a fast growth mechanism beyond a meter in size to avoid destruction. Solutions to this "meter-barrier problem" have been proposed (e.g. Boley et al. 2014), however no clear consensus has yet emerged.

In the gravitational instability model, as the solar nebula cools dust particles settle in the mid plane, becoming vulnerable to collapse (Goldreich & Ward 1973). These dust particles eventually become gravitationally unstable and form $\sim$100m bodies (Goldreich & Ward 1973). The process then repeats again, forming larger and larger planetesimals each time there is a gravitational instability. This model is attractive since it bypasses the scales most vulnerable to destructive collisions (i.e. the meter-barrier problem), and can form large planetesimals in $\sim 10^3$ years (Goldreich & Ward 1973; Armitage 2007). However, in practice it is very difficult to collect dust particles in densities high enough for gravitational instability (Armitage 2007), and especially so in turbulent disks.

The formation mechanism of planetesimals is still unclear, however, *some* mechanism must exist since planetesimals are ubiquitous in the universe.

3. Formation of Protoplanets

The formation of protoplanets occurs shortly after the formation of large, kilometer-sized planetesimals. In a pioneering study, Greenberg et al. (1978) found that in the early stage of planet formation, larger planetesimals grow more rapidly than smaller ones, resulting in the runaway growth of the largest planetesimal. As a result, 1-10km sized planetesimals at 1AU can grow into 10^22 – 10^24kg protoplanets in 10^5–10^6 years (Wetherill & Stewart 1989). This process is initiated by the fact that 1–10km sized planetesimals are large enough to gravitational focus each other yet are still dynamically cool from the surrounding gas, resulting in maximum collision cross sections (Armitage 2010). Since growth time is related to orbital frequency, more distant regions will have slower runaway timescales.

Eventually, this runaway growth will transition into a slower, "oligarchic" growth. As protoplanets grow surrounding planetesimals are dynamically excited via gravitational stirring, decreasing the collision cross section and slowing the rate of protoplanetary growth (Kokubo & Ida 1998). By the end of oligarchic growth, protoplanets have consumed most of the surrounding material, reaching their isolation mass (Schlichting 2014). In the outer parts of a protoplanetary disk the isolation mass is roughly the mass of Neptune, however in the inner regions the isolation mass is a fraction of an Earth mass (Schlichting 2014). Since numerous Kepler planets larger than Earth reside close to their host star, this suggests that either giant impacts between protoplanets or migration must have taken place.

4. Planetary Dynamics

4.1. Mean Motion Resonance

Mean motion resonance (MMR) occurs when the orbital period of one planet is an integer ratio of another. Like other types of resonances occuring in nature, MMR results in the amplitude growth of various quantities characterizing the system like eccentricity, semi-major axis and the longitude of pericentre (Murray & Dermott 1999). As a result, the presence of MMR can strongly affect the formation, evolution and longterm stability of planetary systems in a diversity of ways. For example, Kirkwood gaps are unstable regions in the asteroid belt carved by MMRs with Jupiter, while Pluto and Neptune are protected from going unstable due to a 3:2 MMR.

For every $p : q$ MMR (where p and q are integers) there are two important resonant angles:

$$\begin{aligned} \phi_1 &= p\lambda_1 - q\lambda_2 + \varpi_1 \\ \phi_2 &= p\lambda_1 - q\lambda_2 + \varpi_2 \end{aligned} \tag{9}$$

where λ is the mean longitude and ϖ is the longitude of periapse. For planets in MMR the time variation of one or both of these resonant arguments must be zero. As a result, MMRs can be modelled in terms of a pendulum oscillating about a stable, fixed point. After some algebra it can be shown that a MMR can be modelled as (Murray & Dermott 1999):

$$\ddot{\phi} = -\omega_0^2 \sin\phi \tag{10}$$

where ω_0 is the amplitude of libration and is dependent upon the orbital parameters of the system (mass, eccentricity, semi-major axis).

The pendulum model facilitates understanding about certain properties of MMR. For energies larger than a critical energy E_{crit}, the pendulum will circulate over all possible

values of ϕ, while for energies smaller than E_{crit} the pendulum will be in MMR and librate about $\phi = 0$. The critical energy, E_{crit}, defines motion on the separatrix, which separates the circulation and libration regimes. In context of a pendulum, this would correspond to the pendulum suspended vertically in the air with an infinite period of libration.

The strength of a given MMR is related to its width, which in turn is related to the order of the resonance ($= p - q$) and the magnitude of p and q (Murray & Dermott 1999). More fundamentally, the strength of a MMR is related to the mass, eccentricity and mean motions of the planets involved (Murray & Dermott 1999). Stronger MMRs are associated with lower values of p, q and $p - q$, making the 2:1 and 3:2 MMRs the most probable resonant locations in nature. Figure 1 shows the distribution of period ratios for planets discovered by *Kepler*, along with the locations of first and second order MMRs. As can be seen, statistical excesses of planets exist near the 3:2 and (marginally) 2:1 MMRs (Lissauer et al. 2011; Fabrycky et al. 2014; Steffen & Hwang 2015), supporting the idea that these resonances are most capable of trapping planets.

Planets from these statistical pileups are typically a few percent away from exact period commensurability, and dissipative mechanisms have been proposed to transport these planets from exact MMR. The most popular of these mechanisms are tidal (Lithwick & Wu 2012; Batygin & Morbidelli 2013; Delisle et al. 2014), protoplanetary (Rein 2012; Baruteau & Papaloizou 2013; Goldreich & Schlichting 2014), and planetesimal (Moore et al. 2013; Chatterjee & Ford 2015). The formation implications for each mechanism are different, and no clear consensus has yet emerged.

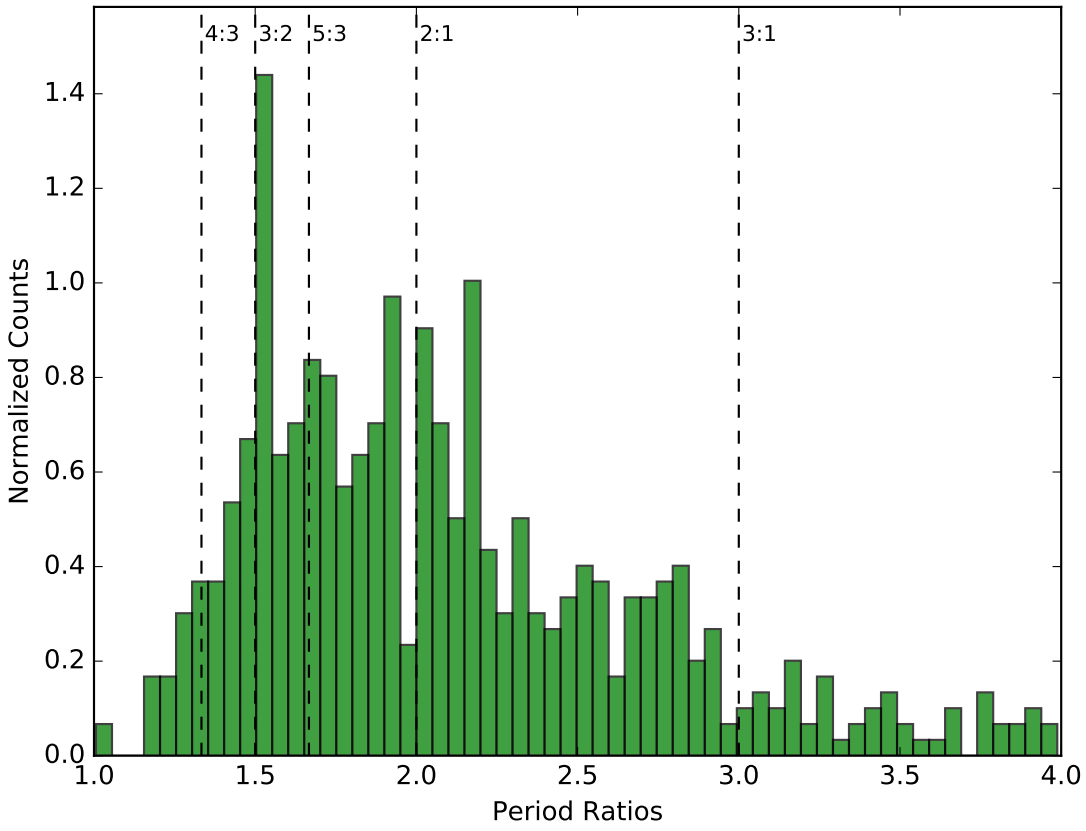

Fig. 1.— Period ratios of neighbouring planets in all known multi-planet systems. Data from NASA Exoplanet Archive (2017). First and second-order mean motion resonances are displayed as dotted lines, and labelled at the top of the figure.

4.2. Migration

4.2.1. Planetesimal-Driven Migration

Planetesimals passing through the Hill sphere of a planet will exchange angular momentum via gravity (Ida et al. 2000; Kirsh et al. 2009). If there is an asymmetry to the number of planetesimals interacting with the planet on its near and far sides, a net force will migrate the planet. However, to guarantee migration, planetesimal orbits must decouple from the planet. A massive enough planet (e.g. Jupiter) will directly eject and decouple planetesimals from the system, however if the planet is smaller (e.g. Neptune) planetesimals must decouple by interacting with a neighbouring planet. In addition, for sustained migration the planet must constantly encounter fresh, dynamically cold planetesimals (Gomes et al. 2004).

Since protoplanetary growth is proportional to orbital frequency (Rafikov 2003), planetesimal disks are most likely to exist in the outer reaches of planetary systems where fewer orbital cycles have occurred. In the Solar System, the primordial Kuiper belt is believed to have once been such a planetesimal disk, causing Neptune to migrate outwards into the Kuiper belt and shepherd planetesimals inwards to Jupiter, which subsequently ejected them from the Solar System (Fernandez & Ip 1984). This idea is well supported by observations of the outer Solar System, which show that Pluto, along with a host of smaller bodies, orbit in stable 3:2 MMRs with Neptune (Malhotra 1993, 1995).

4.2.2. Gas-Driven migration

Since the discovery of the first hot Jupiter (Mayor & Queloz 1995), gas-driven migration is believed to play an important role in shaping exoplanetary systems (Lin et al.

1996). Whenever a fully-formed planet is embedded in a protoplanetary disk, angular momentum can be exchanged via disk-planet torques (Goldreich & Tremaine 1980). The result of this exchange is planetary migration, and this scenario is believed to be common to all young planetary systems. Gas-driven migration comes in two main flavours – Type I and Type II.

Type I migration occurs when low-mass planets are fully embedded in a protoplanetary disk and do not significantly perturb the disk structure (Armitage 2010). At particular resonant locations, known as "Linblad resonances", density waves are excited due to gravitational interactions between the planet and disk (Goldreich & Tremaine 1979). These density waves exchange angular momentum with the planet, and migration occurs when the inner and outer disk interact asymmetrically with the planet (Goldreich & Tremaine 1979). In general, the direction of Type-I migration tends to be inwards towards the central star (Ward 1997).

Type II migration occurs when high-mass Jovian planets significantly modify the structure of the surrounding protoplanetary disk, opening up a gap. This gap locks the planet in place, coupling the migration of the planet to the evolution of the disk (Lin & Papaloizou 1986). The viscous evolution of the disk causes the planet to slowly migrate inwards, at speeds typically one or two orders of magnitude slower than Type-I migration (Ward 1997).

In comparison to planetesimal migration, gas-driven migration is still not well understood. In particular, standard calculations of gas-driven migration are too quick by 1-2 orders of magnitude (Lin & Papaloizou 1986; Tanaka et al. 2002), causing planets to spiral into their central stars before the protoplanetary disk has dispersed. In contrast to this standard view, recent work (Fung & Chiang 2017) has suggested that planets actually do not migrate that much and tend to be better behaved than originally believed.

A consensus on migration has yet to be established, but it is clear that some form of migration must occur in the universe due to the large number of planets in or near MMR (Lissauer et al. 2011; Fabrycky et al. 2014; Steffen & Hwang 2015).

4.3. Stability

The longterm stability of planetary orbits has been studied for hundreds of years by the likes of Issac Newton, Joseph-Louis Lagrange and Carl Friederich Gauss. However, due to the chaotic and non-integrable nature of planetary systems it has been historically difficult to make progress on N-body problems. The chaos in planetary systems is caused by overlapping resonances (Chirikov 1979; Lecar et al. 2001), resulting in the divergence of near-identical systems on long timescales. However, with the aid of computers the equations of motion governing planetary systems can be brute-force integrated into the future or past, allowing scientists to answer fundamental questions that have plagued humans for hundreds of years. For example, it is now known that the Solar System is marginally stable (Sussman & Wisdom 1988; Laskar 1994; Lecar et al. 2001), with Mercury having a 1% chance of colliding with Venus or the Sun within a couple billion years (Laskar & Gastineau 2009). It is also now well established that most known multi-planet systems are packed to capacity, and adding additional planets into these systems would result in dynamical instabilities (Fang & Margot 2013; Pu & Wu 2015).

Although most planetary systems cannot be analytically solved, constraints on these systems can still be derived using analytical means. For example, Wisdom (1980) and Duncan et al. (1989) showed that for small eccentricities in the Restricted 3-Body Problem (R3BP), chaotic orbits (leading to close encounters, collisions and ejections) will occur when the perturber and particle are separated by $\Delta a \leq 1.3\mu_p^{2/7} a_p$ (where subscript p indicates the perturber). Also associated with the R3BP is the Jacobi constant, which can

be used to constrain the chaotic motion of a particle in parameter space. For two massive planets, Gladman (1993) showed that orbits are Hill stable if $\Delta a \geq 3.46 R_H$ (where R_H is the mutual Hill radius), forbidding close encounters for all time.

Since the discovery of numerous exoplanetary systems via *Kepler*, longterm stability has become a popular way to constrain orbital parameters (Lissauer et al. 2011; Steffen et al. 2013; Jontof-Hutter et al. 2014; Tamayo et al. 2015). If one assumes that an observed system is stable over billions of years, grids of N-body integrations can be used to find stable regions of parameter space, further narrowing the range of valid solutions originally constrained by observations. Although this brute-force method is certainly useful, it is not without its costs. A 10 billion year integration or the Solar System takes weeks to complete, and due to the chaotic nature of planetary systems hundreds to thousands of realizations must be simulated to acquire statistically rigorous results.

5. Numerical Integration

5.1. Hamiltonian Dynamics

The Hamiltonian $\mathcal{H}$ encodes the kinetic and potential energy for a system of N bodies. In its most basic form, the Hamiltonian is:

$$\mathcal{H} = \sum_{i=0}^{N-1} \frac{\mathbf{p}_i^2}{2m_i} - \sum_{i=0}^{N-1} \sum_{j=i+1}^{N-1} \frac{G m_i m_j}{|\mathbf{r}_i - \mathbf{r}_j|} \tag{11}$$

where $\mathbf{r}_i$, $\mathbf{p}_i$ and m_i are the position, momentum and mass of body i, respectively. The first term in Equation 11 sums the kinetic energies of the system, while the second term sums the potential energies of the system.

The coordinates ($\mathbf{r}$,$\mathbf{p}$) used in Hamiltonian mechanics are canonical, obeying the

fundamental Poisson bracket relations:

$$\{\mathbf{r}_i, \mathbf{r}_j\} = 0, \qquad \{\mathbf{p}_i, \mathbf{p}_j\} = 0, \qquad \{\mathbf{r}_i, \mathbf{p}_j\} = \delta_{ij} \tag{12}$$

A primary benefit of the Hamiltonian framework is the ease in evolving a N-body system into the future or past via Hamilton's equations:

$$\begin{aligned} \frac{d\mathbf{p}}{dt} &= -\frac{\partial H}{\partial \mathbf{r}} \\ \frac{d\mathbf{r}}{dt} &= \frac{\partial H}{\partial \mathbf{p}} \end{aligned} \tag{13}$$

Numerically this is trivial to do, with the accuracy of the result being inversely proportional to the size of the timestep, dt. A second benefit is the inherent "area preserving" or symplectic nature of Hamiltonian systems, where the energy error is bound to a finite value (excluding e.g. roundoff errors which grow with time).

In the context of planetary systems Equation 11 can be modified to make the evolution more efficient. For example, we know that a planet will orbit in a Keplerian fashion around a central star, determined by the planet's orbital parameters and stellar mass. In multi-planet systems gravitational interactions between planets will occur, perturbing planets off their original Keplerian trajectories. As a result, the Hamiltonian can be restructured into a "Keplerian" term, $\mathcal{H}_K$, and "Interaction" term, $\mathcal{H}_I$ according to (Wisdom & Holman 1991):

$$\mathcal{H} = \mathcal{H}_K + \mathcal{H}_I$$

If the planets are well separated these gravitational interactions are small, and numerically the system can be evolved by applying Keplerian and Interaction operators in a "leapfrog" manner:

$$E_{\mathcal{H}}(dt) = E_{\mathcal{H}_K}(dt/4) \cdot E_{\mathcal{H}_I}(dt/2) \cdot E_{\mathcal{H}_K}(dt/4) \tag{14}$$

where $E_X(Y)$ represents the evolution of the system under X for time Y. Equation 14 is a second order evolution scheme, and is the most popular choice for integrating planetary systems.

5.2. Coordinate Systems

As mentioned above the most efficient way to solve the N-body problem is to split the Hamiltonian into Keplerian and Interaction components. In general, the Keplerian and Interaction Hamiltonians take the following form:

$$\mathcal{H}_K = \sum_{i=1}^{N} \frac{\mathbf{p}_i^2}{2m_i} - \frac{Gm_0m_i}{\mathbf{r}_i}, \qquad \mathcal{H}_I = \sum_{i=1}^{N} \sum_{j=1, j\neq i}^{N} \frac{Gm_im_j}{|\mathbf{r}_i - \mathbf{r}_j|} \tag{15}$$

However, there are numerous ways to perform these splits, with each coordinate system having different strengths and weaknesses. The most popular splittings are are discussed below. In all cases **r** and **p** represent cartesian position and momenta, respectively, N is the total number of particles, and M is the total mass of the system.

5.2.1. Jacobi

Carl Jacobi worked out a coordinate system in which the planet positions are measured relative to the centre of mass of all bodies interior to it. Since a planet's semi-major axis (and hence position) is dependent upon the mass interior to it by Kepler's 3rd law, the evolution of a particle is affected by all bodies interior to it.

The Jacobi position $\mathbf{r}'$ and momentum $\mathbf{p}'$ are a canonical set and are related to the cartesian position and momentum according to (Murray & Dermott 1999):

$$\mathbf{r}'_i = \mathbf{r}_i - \mathbf{R}_{i-1}, \qquad \mathbf{p}'_i = \frac{\eta_{i-1}}{\eta_i}\mathbf{p}_i - \frac{m_i}{\eta_i}\sum_{j=0}^{i-1}\mathbf{p}_j \tag{16}$$

where $\mathbf{R}_i = \frac{1}{\eta_i}\sum_{j=0}^{i} m_j\mathbf{r}_j$ is the centre of mass of all particles interior to body i and $\eta_i = \sum_{j=0}^{i} m_i$ is the sum of masses interior to body i. For the special case of $i = 0$:

$$\mathbf{r}'_0 = \mathbf{R}_N, \qquad \mathbf{p}'_0 = \sum_{j=0}^{N}\mathbf{p}_j \tag{17}$$

The inverse transformations from Jacobi coordinates to cartesian coordinates can be found in Chapter 9.5 of Murray & Dermott (1999).

The benefit of Jacobi coordinates is that the kinetic terms remain a sum of squares (Plummer 1918), making numerical integration a straightforward process according to Equation 14. In addition, these coordinates solve the Two Body and Restricted Three Body Problems exactly. However, the primary disadvantage is that a clear ordering of bodies must be present. For example, in a planetesimal disk orbits cross frequently, and there is no straightforward and (computationally) cheap way to order these bodies.

5.2.2. Democratic Heliocentric

In this coordinate system, positions **Q** and momenta **P** form a canonical set with **Q** measured relative to the central mass and **P** measuring barycentric momenta. These coordinates are related to the cartesian position and momenta according to (Duncan et al. 1998):

$$\mathbf{Q}_i = \mathbf{r}_i - \mathbf{r}_0, \qquad \mathbf{P}_i = \mathbf{p}_i - \frac{m_i}{M}\sum_{j=0}^{N}\mathbf{p}_j \tag{18}$$

For the special case of $i = 0$:

$$\mathbf{Q}_0 = \frac{1}{M}\sum_{j=0}^{N} m_j\mathbf{r}_j, \qquad \mathbf{P}_0 = \sum_{j=0}^{N}\mathbf{p}_j \tag{19}$$

The benefit of Democratic Heliocentric coordinates is that they are easy to understand and do not require the knowledge of other bodies to derive their coordinates (unlike Jacobi coordinates). However, these coordinates do not solve the Two Body Problem or Restricted Three Body Problems exactly. In addition, $\mathcal{H}_K$ cannot be cleanly written as shown in Equation 15 due to several cross terms that arise when substituting (**Q**,**P**) for (**r**,**p**). However, this problem can be rectified by transferring these cross terms into an

additional "Jump" Hamiltonian:

$$\mathcal{H}_J = \frac{1}{2m_0} \left| \sum_{i=1}^{N} \mathbf{P}_i \right|^2 \tag{20}$$

Therefore, the evolution of $\mathcal{H}$ in Equation 14 must be modified to include an additional evolution operator under the Jump Hamiltonian, $E_{\mathcal{H}_J}$. Note that since $\{\mathcal{H}_J, \mathcal{H}_I\} = 0$, the ordering of $E_{\mathcal{H}_I}$ and $E_{\mathcal{H}_J}$ does not matter.

5.2.3. WHDS

The WHDS is a modification of the Democratic Heliocentric mapping that splits the kinetic energy slightly differently. The canonical coordinates **Q** and **P** have the same form, but the Keplerian, Interaction and Jump steps are now (Laskar & Robutel 1995; Wisdom 2006; Hernandez & Dehnen 2016):

$$\begin{aligned} \mathcal{H}_K &= \sum_{i=1}^{N} \frac{\mathbf{P}_i^2}{2\mu_i} - \frac{G(m_0 + m_i)\mu_i}{\mathbf{Q}_i} \\ \mathcal{H}_I &= \sum_{i=1}^{N} \sum_{j=1, j\neq i}^{N} \frac{G m_i m_j}{|\mathbf{Q}_i - \mathbf{Q}_j|} \\ \mathcal{H}_J &= \sum_{i=1}^{N} \sum_{j=1, j\neq i}^{N} \frac{\mathbf{P}_i \cdot \mathbf{P}_j}{m_0} \end{aligned} \tag{21}$$

where $\mu \equiv m_i m_0/(m_0 + m_i)$.

The benefit of these coordinates is that, unlike Democratic Heliocentric coordinates, the Two Body and Restricted Three Body Problems are now solved exactly. In addition, like Democratic Heliocentric coordinates, the coordinates of each particle are independent of all other particles. One price to pay for these benefits is that $\{\mathcal{H}_J, \mathcal{H}_I\} \neq 0$, and in Equation 14 $E_{\mathcal{H}_J}$ must be exactly nestled in between the $E_{\mathcal{H}_K}$ and $E_{\mathcal{H}_I}$ operators. In addition, the standard symplectic correctors of Wisdom (2006) cannot be used in this coordinate system, however other correctors may be possible to construct.

5.3. Integrator Types

The three main classes of N-body integrators are symplectic, non-symplectic and hybrid. Symplectic integrators employ a fixed timestep, bounded energy error (excepting roundoff errors which grow with time) and fast integration time. These integrators are best suited for well-separated bodies where $\mathcal{H}_I \ll \mathcal{H}_k$, otherwise the energy error increases dramatically or the timestep must be changed, both of which break symplecticity. The most popular symplectic integrator is the Wisdom-Holman mapping (Wisdom & Holman 1991).

Non-symplectic integrators do not require a fixed timestep and do not have a bounded energy error over time. However, these integrators can employ very accurate and precise numerical convergence schemes, for example the Burlish-Stoer or predictor-corrector algorithms (Press et al. 2002). As a result, non-symplectic integrators are typically more accurate but slower than their symplectic counterparts, and can solve most classes of planetary physics problems. A popular non-symplectic integrator is `IAS15` (Rein & Spiegel 2015).

Hybrid integrators typically mix the symplectic and non-symplectic schemes, applying the symplectic scheme on bodies that are distant and non-symplectic scheme on bodies that are close. However, there are hybrid schemes that purely rely on symplectic principles (Duncan et al. 1998). As a result, hybrid integrators are often an optimal balance between speed and accuracy, especially for problems involving close encounters. The most popular hybrid integrator is `Mercury` (Chambers 1999).

6. This Work

REFERENCES

Armitage, P. J. 2007, ArXiv Astrophysics e-prints, astro-ph/0701485

—. 2010, Astrophysics of Planet Formation, 294

Baruteau, C., & Papaloizou, J. C. B. 2013, ApJ, 778, 15

Batalha, N. M., Rowe, J. F., Bryson, S. T., et al. 2013, ApJS, 204, 24

Batygin, K., & Morbidelli, A. 2013, AJ, 145, 10

Beaugé, C., Ferraz-Mello, S., & Michtchenko, T. A. 2007, Planetary Masses and Orbital Parameters from Radial Velocity Measurements, ed. R. Dvorak, 1

Blum, J., & Wurm, G. 2008, ARA&A, 46, 21

Boley, A. C., Morris, M. A., & Ford, E. B. 2014, ApJ, 792, L27

Brown, T. M., Latham, D. W., Everett, M. E., & Esquerdo, G. A. 2011, AJ, 142, 112

Chambers, J. E. 1999, MNRAS, 304, 793

Charbonneau, D., Brown, T. M., Latham, D. W., & Mayor, M. 2000, ApJ, 529, L45

Chatterjee, S., & Ford, E. B. 2015, ApJ, 803, 10

Chirikov, B. 1979, Physics Review, 52, 263

Choquet, É., Perrin, M. D., Chen, C. H., et al. 2016, ApJ, 817, L2

Delisle, J.-B., Laskar, J., & Correia, A. C. M. 2014, AA, 566, 14

Duncan, M., Quinn, T., & Tremaine, S. 1989, Icarus, 82, 402

Duncan, M. J., Levison, H. F., & Lee, M. H. 1998, AJ, 116, 2067

Fabrycky, D. C., Lissauer, J. J., Ragozzine, D., Rowe, J. F., & Steffen, J. H. 2014, ApJ, 790, 12

Fang, J., & Margot, J.-L. 2013, ApJ, 767, 115

Fernandez, J. A., & Ip, W.-H. 1984, Icarus, 58, 109

Fressin, F., Torres, G., Charbonneau, D., et al. 2013, ApJ, 766, 81

Fung, J., & Chiang, E. 2017, ArXiv e-prints, arXiv:1701.08161

Gladman, B. 1993, Icarus, 106, 247

Goldreich, P., & Schlichting, H. E. 2014, AJ, 147, 32

Goldreich, P., & Tremaine, S. 1979, ApJ, 233, 857

—. 1980, ApJ, 241, 425

Goldreich, P., & Ward, W. R. 1973, ApJ, 183, 1051

Gomes, R. S., Morbidelli, A., & Levison, H. F. 2004, Icarus, 170, 492

Greenberg, R., Hartmann, W. K., Chapman, C. R., & Wacker, J. F. 1978, Icarus, 35, 1

Hayashi, C. 1981, Progress of Theoretical Physics Supplement, 70, 35

Henry, G. W., Marcy, G., Butler, R. P., & Vogt, S. S. 1999, IAU Circ., 7307

Hernandez, D. M., & Dehnen, W. 2016, ArXiv e-prints, arXiv:1612.05329

Ida, S., Bryden, G., Lin, D. N. C., & Tanaka, H. 2000, ApJ, 534, 428

Jontof-Hutter, D., Lissauer, J. J., Rowe, J. F., & Fabrycky, D. C. 2014, ApJ, 785, 15

Kirsh, D. R., Duncan, M., Brasser, R., & Levison, H. F. 2009, Icarus, 199, 197

Kokubo, E., & Ida, S. 1998, Icarus, 131, 171

Kreidberg, L., Bean, J. L., Désert, J.-M., et al. 2014, Nature, 505, 69

Laskar, J. 1994, A&A, 287, L9

Laskar, J., & Gastineau, M. 2009, Nature, 459, 817

Laskar, J., & Robutel, P. 1995, Celestial Mechanics and Dynamical Astronomy, 62, 193

Lecar, M., Franklin, F. A., Holman, M. J., & Murray, N. J. 2001, ARA&A, 39, 581

Lin, D. N. C., Bodenheimer, P., & Richardson, D. C. 1996, Nature, 380, 606

Lin, D. N. C., & Papaloizou, J. 1986, ApJ, 309, 846

Lissauer, J. J., Ragozzine, D., Fabrycky, D. C., Steffen, J. H., & Ford, E. B. 2011, ApJ, 197, 26

Lithwick, Y., & Wu, Y. 2012, ApJ, 756, 5

Malhotra, R. 1993, Nature, 365, 819

—. 1995, AJ, 110, 420

Mayor, M., & Queloz, D. 1995, Nature, 378, 355

Moore, A., Hasan, I., & Quillen, A. C. 2013, MNRAS, 432, 7

Murray, C. D., & Dermott, S. F. 1999, Solar system dynamics

NASA Exoplanet Archive. 2017, Nasa Exoplanet Archive

Petigura, E. A., Howard, A. W., & Marcy, G. W. 2013, Proceedings of the National Academy of Science, 110, 19273

Plummer, H. C. K. 1918, An introductory treatise on dynamical astronomy

Press, W. H., Teukolsky, S. A., Vetterling, W. T., & Flannery, B. P. 2002, Numerical recipes in C++ : the art of scientific computing

Pu, B., & Wu, Y. 2015, ApJ, 807, 44

Rafikov, R. R. 2003, AJ, 125, 942

Rein, H. 2012, MNRAS, 427, 5

Rein, H., & Spiegel, D. S. 2015, MNRAS, 446, 1424

Sasselov, D. D., & Lecar, M. 2000, ApJ, 528, 995

Schlichting, H. E. 2014, ApJ, 795, L15

Schneider, G., Grady, C. A., Hines, D. C., et al. 2014, AJ, 148, 59

Steffen, J. H., & Hwang, J. A. 2015, MNRAS, 448, 16

Steffen, J. H., Fabrycky, D. C., Agol, E., et al. 2013, MNRAS, 428, 1077

Stevenson, K. B., Bean, J. L., Seifahrt, A., et al. 2016, ApJ, 817, 141

Sussman, G. J., & Wisdom, J. 1988, Science, 241, 433

Tamayo, D., Triaud, A. H. M. J., Menou, K., & Rein, H. 2015, ApJ, 805, 100

Tanaka, H., Takeuchi, T., & Ward, W. R. 2002, ApJ, 565, 1257

Tsiaras, A., Rocchetto, M., Waldmann, I. P., et al. 2016, ApJ, 820, 99

Ward, W. R. 1997, Icarus, 126, 261

Weidenschilling, S. J. 1977a, MNRAS, 180, 57

—. 1977b, Ap&SS, 51, 153

Wetherill, G. W., & Stewart, G. R. 1989, Icarus, 77, 330

Wisdom, J. 1980, AJ, 85, 1122

—. 2006, AJ, 131, 2294

Wisdom, J., & Holman, M. 1991, AJ, 102, 1528

This manuscript was prepared with the AAS LaTeX macros v5.2.